Journal of Power Sources 195 (2010) 4222–4233

Contents lists available at ScienceDirect

Journal of Power Sources

journal homepage: www.elsevier.com/locate/jpowsour

Feedback control of solid oxide fuel cell spatial temperature variation

Mahshid Fardadi, Fabian Mueller*, Faryar Jabbari

Department of Mechanical and Aerospace Engineering, University of California, Irvine, CA 92697, United States

ARTICLE INFO

Article history:
Received 13 November 2009
Received in revised form
19 December 2009
Accepted 22 December 2009
Available online 13 January 2010

Keywords:
Solid oxide fuel cell
Spatial temperature control
H-infinity
Dynamic modeling
Disturbance rejection
Load following

ABSTRACT

A high performance feedback controller has been developed to minimize SOFC spatial temperature variation following significant load perturbations. For thermal management, spatial temperature variation along SOFC cannot be avoided. However, results indicate that feedback control can be used to manipulate the fuel cell air flow and inlet fuel cell air temperature to maintain a nearly constant SOFC electrode electrolyte assembly temperature profile. For example temperature variations of less than 5 K are obtained for load perturbations of ±25% from nominal. These results are obtained using a centralized control strategy to regulate a distributed temperature profile and manage actuator interactions. The controller is based on H-infinity synthesis using a physical based dynamic model of a single co-flow SOFC repeat cell. The model of the fuel cell spatial temperature response needed for control synthesis was linearized and reduced from nonlinear model of the fuel cell assembly. A single 11 state feedback linear system tested in the full nonlinear model was found to be effective and stable over a wide fuel cell operating envelope (0.82–0.6 V). Overall, simulation of the advanced controller resulted in small and smooth monotonic temperature response to rapid and large load perturbations. This indicates that future SOFC systems can be designed and controlled to have superb load following characteristic with less than previously expected thermal stresses.

1. Introduction and background

There is much interest in the shift from fossil fuel to renewable based energy infrastructures to secure energy supplies and reduce environmental impacts (for example see [1–3]). To maintain reliable and dependable energy generation, with increased contributions from renewable sources, a much larger role for dispatchable generation will be required. High temperature fuel cell systems are an attractive solution with ultra low pollutant emissions and high efficiency—particularly if used in hybrid arrangements. The ability to achieve high efficiencies on smaller scales opens the door for distributed generation and use of renewable biogas. To fully exploit the benefits of this new paradigm, the fuel cell must have a relatively large envelop of transient operation (changes in power demand or the supply of renewable fuel).

High temperature fuel cells are currently being deployed as base-loaded system as the technology is slowly overcoming the many engineering challenges to be competitive in the market place. In particular, transient operation of SOFC system can be very attractive. Simulations indicate that well designed integrated SOFC systems can load follow very rapidly [4–9]. The current drawn from SOFC can be increased at the rate of electrochemistry, on the order of milliseconds, with increased efficiency at part load, and ultra low pollutant emissions for the whole range of operation (see [10] for a list of SOFC attributes).

A major issue inhibiting transient SOFC operation is that thermal stresses during transient operation can increase the probability of failure and degradation of the fuel cell (e.g., see [11–14]). To minimize thermal stresses and the corresponding probability of failure, it is critical to minimize spatial temperature variations during SOFC operation. The goal of this paper is to evaluate the ability to minimize fuel cell spatial temperature variations, during transients.

Transient operation of solid oxide fuel cell requires advanced integrated system controls as explored in [4,7,9,15,16] to maintain the system within operating requirements. Exact SOFC system controller design can vary depending on the SOFC system design and configuration. However, all fuel cell systems will generally require a (1) system power controller, (2) a fuel utilization/combustor temperature controller, and (3) a fuel cell stack temperature controller. The first two have received ample attention, for example see [4,5,7,16,17]. The focus of this paper is on spatial temperature control. Since fuel cell temperature response time constants are considerably larger than fuel and electrochemical response and different actuators are used for fuel, electrochemical and temperature control, it is possible to decouple fuel cell temperature control from the more rapid fuel flow and fuel cell current control.

Fuel cells are thermally managed by control of air through the fuel cell. Temperature increase in the air flow direction of the fuel

* Corresponding author. Tel.: +1 949 824 6602; fax: +1 949 824 7423.
E-mail address: fm@apep.uci.edu (F. Mueller).

0378-7753/$ – see front matter © 2010 Elsevier B.V. All rights reserved.
doi:10.1016/j.jpowsour.2009.12.111

Nomenclature

C	solid specific heat capacity [kJ kg^{-1} K^{-1}]
C_V	constant volume gas specific heat capacity
E	voltage polarization [V]
F	Faradays constant [96,487 C mol^{-1}]
h	enthalpy [kJ kmol^{-1}]
h_f	enthalpy of formation [kJ kmol^{-1}]
i	current [A]
N	molar capacity [kmol]
$\dot{N}$	molar flow rate [kmol s^{-1}]
Nu	Nusselt number [–]
P	pressure [kpa], power [kW]
ρ	density of solid [kg m-2]
$\dot{Q}$	heat transfer [kW]
R	species reaction rate [kmol s^{-1}], universal gas constant [8.3145 J mol^{-1} K^{-1}]
t	time [s]
T	temperature [K]
V	volume [m^3], voltage [V]
$\dot{W}$	rate of work [kW]
X	species mole fraction [–]

cell is generally unavoidable and is a critical fuel cell design consideration. The nominal full-power operating SOFC temperature profile is a trade-off between the fuel cell material durability and system efficiency. SOFC are made of thin ceramic tri-layer consisting of a positive electrode, electrolyte, negative electrode (PEN) that can crack due to thermal stresses. However, to maximize system efficiency the fuel cell air flow rate should be minimized resulting in increased temperature gradient and increased thermal stresses within the PEN.

Different stack configurations and fuel cell thermal management strategies exist in the literature (for examples see [18–20]). A single planar fuel cell is considered here, with a 100 K temperature increase in the PEN from 1023 to 1123 K, in balanced or nominal operation. The optimization of the nominal temperature profile is not the focus of the paper, since the nominal temperature profile is application dependent. The control goal here is to minimize variation in the fuel cell PEN spatial temperature in time. This is particularly challenging during load perturbations as the amount of heat generated within the fuel cell changes non-uniformly.

Research has shown that the average temperature of fuel cells can be effectively managed by manipulating the cathode air flow rate through the fuel cell [4–6,21,22]. However, to minimize fuel cell degradation, variations in the fuel cell temperature must be minimized. For example, Nakajo et al. [13,23] have shown that probabilities of failure can increase significantly due to temperature variation during transient. Inui et al. [24] have showed that it is possible to minimize the spatial temperature variations of the fuel cell over a large fuel cell operating envelope by optimally manipulating both the fuel cell air flow and air inlet temperature to minimize temperature variations. That work is based primarily on steady-state analysis and is not directly related to transient operation under changing loads or disturbances. This research builds on the work of Inui et al., to demonstrate the performance of controls to maintain a nominal fuel cell spatial temperature profile, in time, during load perturbations.

A model with modest levels of spatial distribution is utilized herein. Due to the uneven distribution of current and thus heat generation, as well as heat conduction and convection, there can be significant variations in the temperature profile of the fuel cell, along the length of the cell. These large variations can lead to damage or failure and average temperature from a bulk model would not show the extent of the thermal stress. We start by a fuel cell operating at the baseline condition, based on some maximum overall efficiency consideration. We then show the temperature variations from the temperature profile associated with the baseline condition due to disturbances associated with power demand fluctuations. After linearizing the model about the operating conditions, we show the large range of variations that can be captured by the approximate model. Next, we develop high performance controllers that reduce the variations significantly and compare the results with what could have been obtained from extensive simulation and off-line optimization (e.g., look-up tables).

Consistent with the work of Inui et al., the air flow rate and inlet temperature are considered as manipulated variables. In SOFC system, the air flow rate can be varied either by variable speed compressor and blowers (as was explored in [4,5,7,25]) or by air inlet guide vanes (see [25]). The air inlet temperature can be manipulated by bypassing air recuperators. The air flow rate and air inlet temperature can be manipulated independently to minimize spatial temperature variations in time. The results show the potential for use of advance control techniques for high performance operation of fuel cell power systems.

2. Dynamic modeling

Fuel cell temperature control are developed and evaluated using a quasi-dimensional nonlinear dynamic model of a repeated cell within a stack based on transport and conservation principles. The fuel cell dynamic modeling methodology has been used in many previous efforts including [4,5,7,15,25–33] and compared to both cell and system level experimental data [26,28–30,32,33]. Since the focus of the paper is controls, the physical dynamic model is only briefly presented. The simulations are conducted in the Simulink platform to enable ease of use of Matlab control tools. The model is based on conservation of mass, species, and energy along with convective and conductive heat transfer, steam reformation reaction and fuel cell electrochemistry. Due to the broad spectrum of time scales involved (millisecond to hours), time differential equations are solved using Simulink ODE15s built-in stiff system time differential solver. For spatial and temporal resolution the fuel cell is quasi-dimensionally discretized (in 2-D) into five nodes along the flow direction consisting of the PEN tri-layer, interconnect plate, anode, and cathode gas channel control volumes as shown in Fig. 1.

2.1. Model discretization

In total the fuel cell is discretized into 20 control volumes (4 layers per node times 5 nodes in flow direction), where the top and

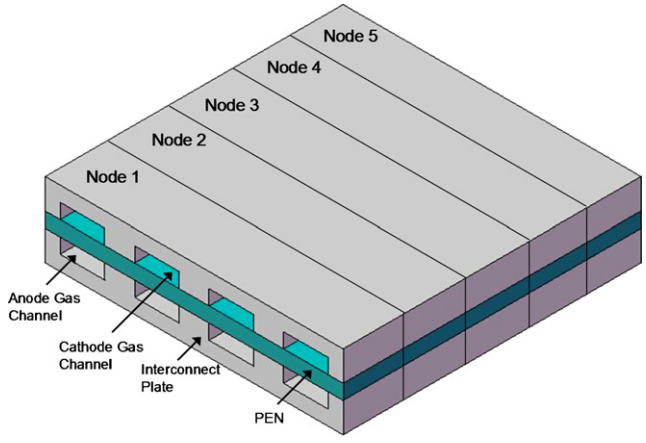

Fig. 1. Quasi 2-dimensional co-flow SOFC spatial discretization.

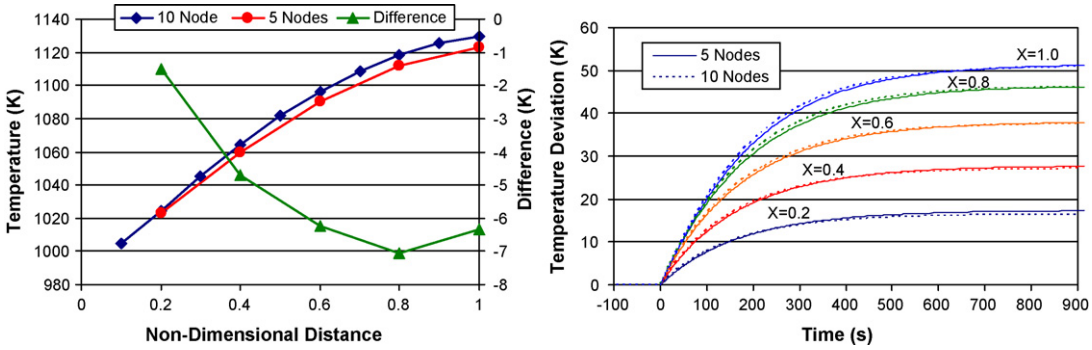

Fig. 2. Discretization sensitivity analysis.

bottom interconnect plate is assumed to be the same resulting in a periodic boundary condition, since in a typical fuel cells large number of cells are stacked next to another. Within each control volume only the physical and chemical processes that affect the time scale of interest in the dynamic simulation are considered (>10 ms). For example, processes such as electrochemical reaction rates and electric current flow dynamics are assumed to occur at a time scale that is faster than that of interest to the model.

The temperature of each control volume as well as methane, carbon monoxide, carbon dioxide, hydrogen, water and nitrogen mole fraction in the anode gas, and nitrogen and oxygen mole fraction in the cathode gas is resolved dynamically. In total the full physical nonlinear model contains 60 states (5 nodes each with 4 temperature, 6 species per anode gas CV, 2 species per cathode gas CV). Compared to other spatial dynamic models in the literature the discretization of the current work is relatively coarse (for example see [12]). The simplicity of the spatial dynamic model is necessary for effective linearization and control development. In fact, the 60 state linear model has to be further reduced for the controller synthesis.

It has been suggested [34] that five nodes is not sufficient to accurately capture the fuel cell spatial temperature distribution. Sensitivity analysis of the fuel cell spatial temperature distribution between a 5 and 10 node model (see Fig. 2) indicates that 5 nodes may result in some inaccuracies in modeling steady-state spatial temperature distribution. However, it was found that the change in temperature at each node due to perturbation is well captured by a 5 node model. For example, the PEN spatial temperature response for a 0.5 V decrease from nominal operating conditions of both the 5 and 10 node model is almost exactly the same (see Fig. 2, right-hand side). The results indicate that while 5 nodes cannot precisely evaluate the temperature profile, a 5 node model can well capture spatial temperature deviation from nominal temperatures for given perturbation and thus is adequate for evaluating how closely SOFC spatial temperature deviations can be minimized in time. As discussed below, many of the 60 states have weak contributions to the input–output characteristics of the fuel cell, particularly for the time scales of interest, and can be eliminated without much effect.

2.2. Model summary

The fuel cell PEN assembly temperature is resolved one dimensionally in the flow direction capturing:

1. Heat generation from electrochemistry.
2. Conduction heat transfer through the PEN assembly.
3. Conduction heat transfer through the metal interconnect.
4. Conduction heat transfer between the PEN and metal interconnect
5. Convection heat transfer to the fuel and air stream.
6. Surface steam reformation and water gas shift chemical reactions.

Conduction heat transfer between the PEN and interconnect plate as well as along the flow direction is modeled by Fourier law. Convective heat transfer between the solids and gas flow are modeled by Newton's law using constant Nusselt number approximation. (See Table 1 for model parameters used e.g., k_{plate}, k_{pen}.) Corresponding energy conservation equation within the PEN control volumes is as follows:

$$\rho V C \frac{dT}{dt} = \sum \dot{Q}_{hx} + \sum \dot{Q}_{react} - \dot{Q}_{elec} \quad (1)$$

$$\dot{Q}_{elec} = -\left(h_{f(H_2O)}(T_e) \cdot \frac{i}{n \cdot F} - iV\right) \quad (2)$$

where $\dot{Q}_{hx}$ is the heat transfer into the control volume, $\dot{Q}_{react}$ is the heat release from the steam reformation and water gas shift reactions, $\dot{Q}_{elec}$ is the heat generated by electrochemistry. The interconnect plate conservation equation is modeled in a similar fashion without the reaction and electrochemical contributions.

Energy and species conservation are applied at each gas channel control volumes as follows:

$$NC_v \frac{dT}{dt} = \dot{N}_{in} h_{in} - \dot{N}_{out} h_{out} + \sum \dot{Q} \quad (3)$$

$$N \frac{d\vec{X}}{dt} = \dot{N}_{in} \vec{X}_{in} - \dot{N}_{out} \vec{X}_{out} + \vec{R} \quad (4)$$

Electrochemical reactions are assumed on the surface of the PEN gas interface based on Faradays law. Steam reformation and water gas shift reaction are also assumed to be uniformly distributed on the surface of each PEN control volume. The water gas shift reaction is assumed to be in equilibrium and steam reformation kinetics are based on Xu and Froment [35,36], using anode gas specie mole

Table 1
Planar SOFC parameters.

	Value	Units	Description
W	0.1	m	Cell width
L	0.1	m	Cell length
t_{plate}	0.001	m	Interconnect plate thickness
Channels	10		Flow channels per cell
$W_{channel}$	0.005	m	Width of flow channels
ρ_{pen}	5000	kg m^{-3}	PEN solid density
ρ_{plate}	7900	kg m^{-3}	Interconnect plate density
C_{pen}	0.8	kJ kg^{-1} K^{-1}	PEN specific heat capacity
C_{plate}	0.64	kJ kg^{-1} K^{-1}	Interconnect plate specific heat capacity
k_{pen}	10×10^{-3}	kW m^{-1} K^{-1}	PEN conduction coefficient
k_{plate}	20×10^{-3}	kW m^{-1} K^{-1}	Interconnect plate conduction coefficient
Nu	4.12		Nusselt number
i_o	4000	A m^{-2}	Fuel cell exchange current density
i_l	9000	A m^{-2}	Fuel cell limiting current density

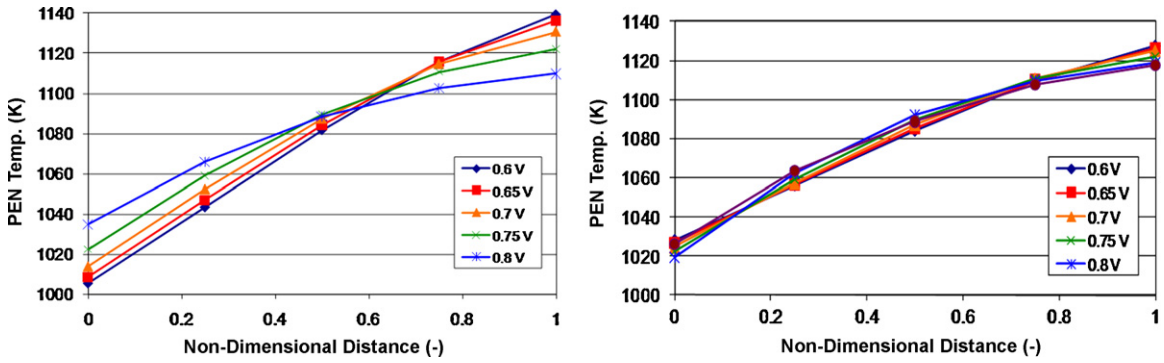

Fig. 3. PEN peak spatial temperature deviation minimization for (a) simple air flow manipulation and (b) air flow and inlet temperature manipulation.

fraction and the PEN solid temperature. This provides discretization of the reformation reactions along the flow channels of the fuel cell.

From gas channel species and PEN temperature, the electrochemical potential at each node is found from the Nernst equation along with Ohmic, activation, and concentration polarization:

$$V_{\text{Nernst}} = -\frac{\Delta G(T)}{n \cdot F} + \frac{R \cdot T}{n \cdot F} \ln\left[\frac{P_{H_2} \cdot {P_{O_2}}^{1/2}}{P_{H_2O}}\right] \quad (5)$$

$$E_{\text{ohm}} = R(T) \cdot i \quad (6)$$

$$E_{\text{act}} = \frac{2 \cdot R \cdot T}{n \cdot F} \sinh^{-1}\left(\frac{2 \cdot i/A}{i_o}\right) \quad (7)$$

$$E_{\text{conc}} = -\frac{R \cdot T}{n \cdot F} \ln\left(1 - \frac{i/A}{i_l}\right) \quad (8)$$

The internal resistance is modeled as a function of temperature from Kim et al. [37]. Since the interconnection plate is metal, all nodes in the fuel cell will have the same voltage. The current that makes each node voltage equal to the cell voltage must be found. However, a closed form equation of node current as a function of voltage does not exist. This represents a minor modeling challenge since to linearize the model for control synthesis, the model cannot have any algebraic loops. To resolve this problem a look-up table of current versus temperature and voltage polarization is created. The total polarization at a node is known from the cell operating voltage and the Nernst equation and the PEN temperature is known from the conservation of energy.

$$E_P(T, i) = V_{\text{Nernst}} - V \quad (9)$$

Therefore, the current at each node can be evaluated without any algebraic loops. However, a look-up table of the voltage polarization must be updated if any of the voltage polarization constant parameters are varied.

3. Control preliminaries

3.1. Steady-state optimization

Due to non-uniform heat release at different fuel cell operating power, a single spatial temperature distribution in the fuel cell cannot be maintained exactly. Before developing a spatial temperature controller it was desired to understand how closely the fuel cell spatial temperature can be maintained at steady state by manipulating the air flow and air inlet temperature of the fuel cell for the specific design.

As a starting point, we use 0.75 V as the nominal voltage for the operating condition. This is a typical value used in based-line operation. Steady-state values for air flow rate and inlet temperatures are obtained so that the fuel cell PEN temperatures at the air inlet and outlet are 1020 and 1120 K, respectively. The voltage is varied from the nominal value, as a proxy for power demand variation. The range of voltage variation is from 0.6 to 0.82 V. As discussed later, this is a significant range, roughly corresponding to ±25% variation in power.

The nonlinear model was used to evaluate optimal air and inlet air temperature to minimize the PEN solid temperature deviation from the nominal 0.75 V temperature profile for a few operating voltages (e.g., 0.6, 0.7). Specifically, the temperature variation at each node was evaluated, and different air flow and inlet temperature were searched to minimize the peak node temperature variation (peak $|T - T_{0.75\,\text{V}}|$). Note that different cost functions (e.g. square of error, etc.) can be used to achieve different optimal spatial temperature profiles. Results from the optimization are presented in Fig. 3 for two cases: one with just air flow manipulation and a second with both air and temperature manipulation.

The steady-state optimization result highlights the importance of having both air flow and air inlet temperature control to thermally manage the fuel cell. With only one actuator the temperature at the exit of the fuel cell will vary by more than 30 K for an operating range between 0.6 and 0.8 V per cell. With independent air flow and air inlet temperature control, each node PEN temperature can be maintained within 8 K for the same operating range.

While the optimization results presented apply only to steady-state conditions, it underlines that having control of both the air flow and air inlet temperature is critical in minimizing fuel cell spatial temperature variations in time, at part load operating conditions. Without dual actuation, the increase air flow rate at higher power causes an increase in the temperature gradient across the fuel cell. This is because the higher flow rate disproportionally cools the inlet of the cell compared to the outlet, resulting in an increase temperature gradient across the fuel cell, which can be highly damaging to the long-term reliability/durability of the cell. To counterbalance this phenomenon, the inlet air temperature can be increased, thereby maintaining the fuel cell spatial temperature distribution. Increasing the air inlet temperature at high power is somewhat counter intuitive. As can be seen from Table 2, the air flow rate is larger at a given voltage in the dual actuation case, when the voltage is dropped (i.e., increase in power and heat generation). Naturally, the air flow rate has to be further increased with increased air inlet temperature. As expected, the situation is reversed when the voltage is increased for lower power (thus lowers heat generation). The optimization results signify that a central controller can be beneficial to manage interactions between air flow and air inlet temperature actuation directly. Hence, a high performance centralized feedback controlled is developed and demonstrated herein to evaluate SOFC transient capability. Note that hereafter, the term 'open loop' refers to control systems without feedback loops while 'closed loop' denotes control systems with output feedback.

Table 2
Deviation (from nominal) minimization: steady-state optimization.

Voltage [V]	Air flow control		Air flow and inlet temperature control	
	Air flow rate [kmol s^{-1}]	Air inlet temperature [K]	Air flow rate [kmol s^{-1}]	Air inlet temperature [K]
0.6	8.39E−06	937.1	1.21E−05	983.9
0.65	7.30E−06	937.1	1.00E−05	978.5
0.7	5.99E−06	937.1	7.45E−06	966.7
0.75	4.49E−06	937.1	4.49E−06	937.1
0.8	2.94E−06	937.1	1.60E−06	808.4

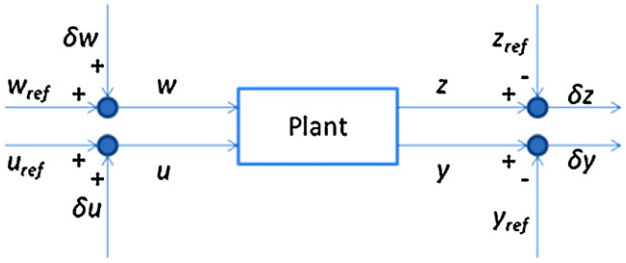

Fig. 4. Linearization block diagram.

3.2. Model linearization

We first attempt to evaluate the feasibility of using a linearized model of the system for the purposes of control design. If successful, this would open the door for a variety of modern and high performance control methods. Here, we first linearize the model and compare the open loop response of the nonlinear system with the linear approximation (and indeed a reduced order linear model). Next, we develop controller for the linear approximation, as discussed below, and verify the feasibility of the overall approach by implementing the controller obtained on the full nonlinear model.

The first step, linearization, is rather straight forward since it can be obtained via the built-in features of MATLAB. For this we allow the nonlinear model (in SIMULINK) to reach steady state, for a given voltage, fuel and airflow, etc. We then obtain the linearized model around this operating condition. Matrices, A, B_1, B_2, C_1, C_2, D_{11}, D_{12}, D_{21}, and D_{22} in (11), below, are the outputs of linearization command of MATLAB.

Now consider the schematic of Fig. 4, when the box 'Plant' refers to the actual nonlinear model, with u_{ref}, y_{ref}, w_{ref}, and z_{ref} the inputs and outputs corresponding to the steady-state nominal conditions. In the absence of disturbances, with inputs u and w being set to u_{ref} and w_{ref} (set-point inputs), the output will match y_{ref} and z_{ref}. As the input is changed (or indeed as the disturbance is introduced) the output will differ from y_{ref} and z_{ref}. The linearization about nominal operating condition results in an approximation of how the outputs differ from nominal values (i.e., δy and δz) due to δu and δw.

In the following $x(t) \in R^n$ denotes the states, $w(t) \in R^{m_1}$ is a vector of exogenous inputs (e.g. external disturbances and noise on the system), $u(t) \in R^{m_2}$ is the vector of control inputs, $z(t) \in R^{p_1}$ is a vector of control variables and $y(t) \in R^{p_2}$ is the measurement vector (sensors).

Deviation of the state, input, and output from their nominal trajectories are indicated by δx, δu, δw and δy (δx represents the change in state, δy represents the change in sensors, δz represents the change in control variables, δu represents the change in control inputs, and δ_w represents the change in disturbances from the steady-state values), as in

$$\begin{aligned} \delta x &= x - x_{\text{ref}} \\ \delta u &= u - u_{\text{ref}} \\ \delta y &= y - y_{\text{ref}} \\ \delta w &= w - w_{\text{ref}} \\ \delta z &= z - z_{\text{ref}} \end{aligned} \tag{10}$$

The resulting model looks like

$$\begin{cases} \dot{\delta x} = A\delta x + B_1\delta w + B_2\delta u \\ \delta z = C_1\delta x + D_{11}\delta w + D_{12}\delta u \\ \delta y = C_2\delta x + D_{21}\delta w + D_{22}\delta u \end{cases} \tag{11}$$

Without loss of generality, D_{22} can be assumed zero in control system design problems. As indicated in [38], by defining a fictitious measured output $\hat{y} = C_2\delta_x + D_{21}\delta_w$ of (2), one can design the controller $u(t)$, and then replace $\hat{y}$ by $\delta y - D_{22}\delta u$. Therefore under assumption of the system being well-posed, we only use Eq. (11) with $D_{22} = 0$.

Once this model is obtained, it may be used in controller design, including techniques that can address multiple inputs and multiple outputs (MIMO) systems with ease, including those with significant cross coupling between different input/output channels. The specific disturbances, actuators, and sensors are listed in Table 3. The physical motivation for the choice of these input and output is as follows: As inputs, we use variables that are typically available for manipulations for temperature control. Therefore the inputs are cathode inlet temperature and air flow rate. Other variable can be used for control purposes; for example current drawn or fuel flow. These, however, are often used for power tracking and other objectives. Here we focus on cathode flow: flow rate controlled by a blower or fan, and inlet air temperature controlled by bypassing a portion of air around air heat exchangers. For disturbances we use common type of disturbances such as fuel cell voltage, fuel composition and anode inlet temperature. The anode outlet temperature, and interconnect plate temperature at the air inlet middle and air outlet are measured output signals (sensors). For sensors we have aimed for a balance between practical considerations (ease of use via thermocouples etc.), proximity, and coupling with key performance objective; reducing the temperature variations from the nominal profile along the fuel cell Finally, for performance (or control) variables (z), the five nodes' PEN temperatures have been used. If there is a need to consider spatial gradient temperature of the fuel cell, the vector z can be augmented to incorporate this concern. For

Table 3
List of inputs and outputs.

Disturbances	(1) Nitrogen dilution (2) Anode inlet temperature (3) Fuel cell voltage
Actuators	(1) Cathode inlet temperature (2) Air flow rate
Sensors	(1) Anode outlet temperature (2) Plate temperature of first node (3) Plate temperature of middle node (4) Plate temperature of last node
Control variables	(1) First node electrolyte temperature (2) Second node electrolyte temperature (3) Third node electrolyte temperature (4) Fourth node electrolyte temperature (5) Fifth node electrolyte temperature

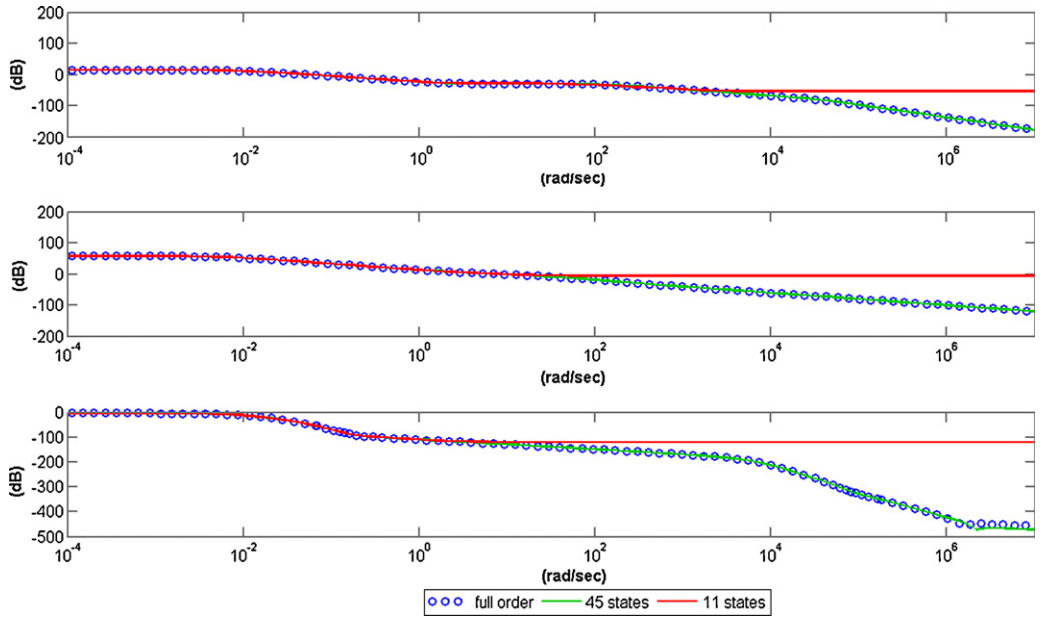

Fig. 5. Bode plots for selected inputs and outputs for full order and reduced order models (top: 1st node temperature of PEN versus nitrogen dilution; middle: 3rd node temperature of PEN versus fuel cell voltage; bottom: 5th node temperature of PEN versus cathode inlet temperature).

example, we can add $\delta T_i - \delta T_{i-1}$ for $i = 2, 3, 4, 5$ to the vector δz as an approximation for the gradient of the temperature along the cell. Effect of different combinations of δz will be discussed in the transient analysis section.

At least five fuel cell nodes must be resolved for control synthesis. However, we have found that measuring three interconnect temperatures provides sufficient information of the PEN temperature being controlled. Note that the controllers uses the 3 interconnect temperature measurements, along with the other sensors and state-space model, to estimate the PEN temperature states. More sensors can add redundancy and slight accuracy improvements, but are generally not required.

3.3. Model reduction

As discussed in the physical model section, the linearized plant has 60 states, corresponding to the states of the nonlinear model. The order of the plant model needs to be reduced to make it less susceptible to numerical error and to reduce computational burden. The reduced order and full order state-space model have the same structure as Eq. (11).

In the first step, unobservable and uncontrollable states have been removed since they do not contribute to the model's input–output behavior. After removing the uncontrollable and unobservable states, the reduced linear model has 45 states. In the second step, the states with the least effect on the system response have been removed. For example: balanced model reduction based on Hankel singular values are used to reduce a large order model by removing states that have weak controllability and/or observability properties and thus do not contribute to input–output (i.e. physical) characteristics [39]. The states with the least effect on the system response (smallest Hankel singular value) were then removed in order of smallest to largest Hankel value, ensuring the linear system's time and frequency response were not substantially affected

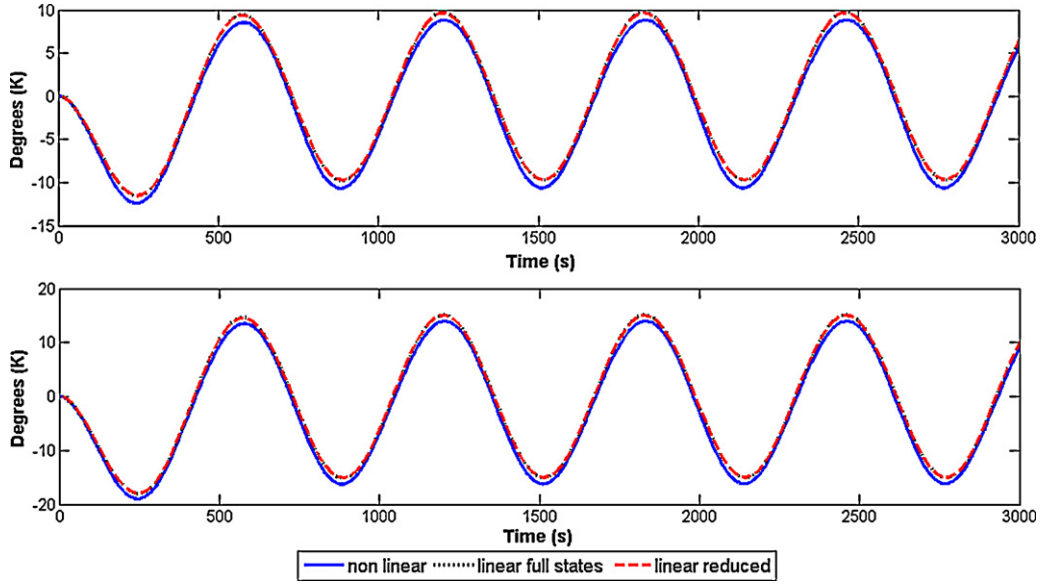

Fig. 6. Temperature variation from nominal due to 10% sinusoidal perturbation in nitrogen mole fraction and fuel cell voltage (top plot: 1st node; bottom plot: second node).

after each removal. In this system the range of Hankel singular values was from very close to zero to 3.97×10^7. Due to a natural, and relatively large, gap in the singular values between about 80 and 500, we chose to keep those above 100, leading to a reduced order model of order 11.

After model reduction, the model contained 11 states with Hankel singular values greater than 10^2. Fig. 5 compares the frequency response for the full state linear model and the reduced order linear models (order 45, and 11). The difference between full order model and reduced order models is not important after 10^2 rad s^{-1}, because temperature response is a slow process. Therefore, the model with 11 states is a good approximation of full order model for our range of frequency.

To further evaluate the effects of linearization and model reduction, the open loop time response of the full order linear, the reduced order linear and the nonlinear models were compared for a representative disturbance. Fig. 6 provides the open loop response of the linearized model, reduced order model and nonlinear system (actual system) to a 10% sinusoidal variation in nitrogen model fraction and voltage.

Fig. 6 indicates that the response predicted by reduced order model matches well the response predicted from the nonlinear model and that perturbations in fuel cell voltage and fuel composition have a substantial effect on the system's operating point, requiring control for disturbance rejection. The large variations of temperature due to load perturbation can lead to thermal fatigue and decrease the life of the fuel cell [13,23]. Note several other bounded disturbances were also tested, all of which lead to similar results. These results are not shown here for the sake of brevity.

4. Feedback control design

In this section, the concepts and definitions used to design controllers are presented. Once a linearized model is available, a variety of control methods can be used. Here we present a controller obtained from a standard H-infinity or L-2 gain approach. This is partly due to the natural match between our objectives: reducing the effects of disturbances on the control outputs, and the temperature profile of the fuel cell [40].

We start with the assumption that due to small variations from the steady-state conditions, the behavior of the plant can be represented by the linear model (see Eq. (11)). We use this linear model to obtain a compensator of the from

$$\begin{cases} \dot{x}_c = A_c x_c + B_c \delta y \\ \delta u = C_c x_c + D_c \delta y \end{cases} \tag{12}$$

Naturally, given the linearization discussed above, the controller (shown schematically in Fig. 7) aims to minimize the effects of disturbances (e.g. changes in fuel composition, and power demand) on the temperature variations from the nominal case (0.75 V for fuel cell voltage and 0.1 for nitrogen dilution). To be precise, the controller minimizes 'γ', which is an estimate for bounding the energy of the output signal, given the energy of disturbance signal

$$\int \delta z^T \delta z \, dt \le \gamma^2 \int \delta w^T \delta w \, dt \tag{13}$$

While, for clarity of exposition, we only discuss the basic L-2 (or energy) gain controllers, the extensions to address a variety of key concerns are readily available. Among these are frequency weighing to focus on appropriate bandwidth (e.g., relatively high frequency for power changes and low ones for fuel composition changes), tracking, robustness to modeling error, incorporating peak minimization features (rather than energy minimization), and multi-objective techniques to account for simultaneous objectives [38–42].

The approach used is, by now, standard [38,40–43]. A controller of the same order as the plant (i.e., dim of A_c is the same as that of A) can be obtained through the use of one of the standard Matlab Tool Boxes (i.e., LMI Tool Box). Details are omitted for brevity but the interested reader can consult references [38,41–44] for more information.

Different choices of inputs and outputs lead to different physical control structures. In some combinations, the resulting controllers (compensators) might not be stable, which would cause difficulties due to presence of disturbance, nonlinearity or numerical error. As a result, in all cases, we check the stability of the controller.

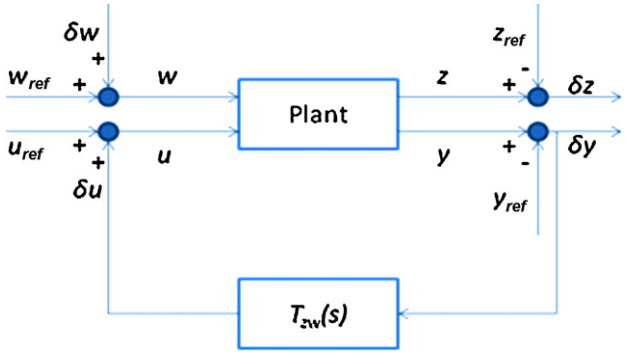

Fig. 7. Feedback control block diagram.

5. Steady state and transient analysis

Based on the input–output information in Table 3, an H-infinity output feedback controller was designed. The optimal value for gamma, the energy gain from input disturbance to the output (see Eq. (13)) for this controller is 126.29, whereas that of the open loop system is 1773.6. To evaluate the efficiency of this controller, we focus on fuel cell voltage disturbance, which is the most critical disturbance (among those studied here), due to its rapid response time (timescale of about seconds). Another reason for selecting voltage disturbance is because of its significant effects on the spatial temperature profile, as illustrated in Fig. 6. To evaluate the overall approach, we introduced changes in the set-point voltage from the nominal (0.75 V) to range from 0.6 to 0.82 V. This range of voltages corresponds to roughly ±25% change in the power, a significant range which is considered beyond the ability of current fuel cells, partly or mostly due to the issue of reliability and thermal fatigue. The change in voltage is implemented as a ramp from 0.75 to 0.82 V with slope of 0.01 V s^{-1} and a ramp from 0.75 to 0.6 V with slope of −0.01 V s^{-1}.

To compare the results of the closed loop system versus open loop system, several simulations were run for voltages between 0.6 and 0.82 V. Table 4 shows variation of the fuel cell power for variation of voltage from 0.6 to 0.82 V and also steady-state temperature error for open loop and close loop systems.

Table 4
Temperature deviation (from nominal): open loop and closed loop.

V (V)	ΔP (%)	$\sum_{i=1}^{5} \lvert\delta T_i\rvert$ Open loop	$\sum_{i=1}^{5} \lvert\delta T_i\rvert$ Closed loop
0.6	26	460.89	20.65
0.65	25.874	330.83	15.94
0.7	18.94	178.09	9.4184
0.75	0	0	0
0.8	−19.16	195.92	13.652
0.82	−28.694	274.83	14.195

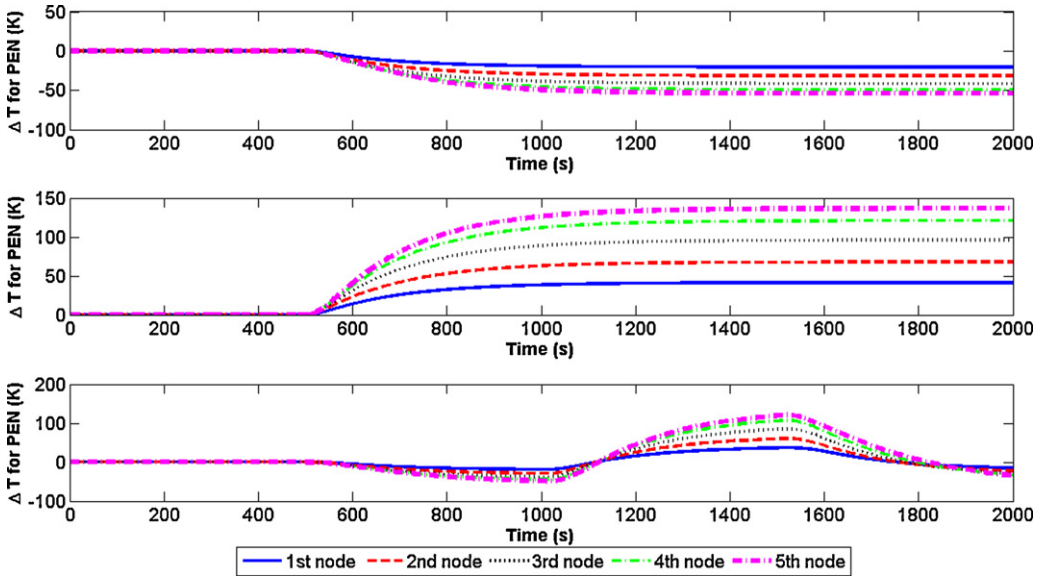

Fig. 8. Open loop temperature deviation from nominal (top: increasing voltage; middle: decreasing voltage; bottom: voltage fluctuation).

The spatial temperature deviation from 0.75 V was evaluated with the ramp function discussed above for the following three different voltage disturbance scenarios:

(i) Voltage increase to 0.8 V at t = 500 s.
(ii) Voltage decrease to 0.6 V at t = 500 s.
(iii) Intermittent voltage variation between 0.6 and 0.8 V every 500 s.

5.1. Open loop results

Fig. 8 demonstrates the spatial temperature response for open loop system. As Fig. 8 shows temperature variations for the five nodes are 20–50 K for increasing the voltage, and 50–150 K for decreasing the voltage. The large temperature variations seen here may be quite damaging to the fuel cell [13,23]. Also note that the temperature gradient is also increased.

5.2. Closed loop results

Fig. 9 illustrates the temperature deviations for increasing voltage and decreasing voltage respectively, under feedback control. H-infinity output feedback controller has been used to minimize fuel cell temperature deviation from the nominal temperature profile by manipulating the inlet air flow rate and cathode inlet temperature from the nominal operating condition. As simulation results indicate (Fig. 9), the temperature variation at each node for changing voltage is less than 6 K.

Fig. 10 shows the actuators behavior during transients for feedback controller. The two top subplots are controller output for increasing voltage and the two bottom subplots are for decreasing voltage. When voltage decreases, power increases, resulting in an increase to the heat generation in the fuel cell. As Figs. 8–10 show the extra heat from the fuel cell has been removed through increasing the air flow rate and cathode inlet temperature. These plots underline the importance of developing a controller that takes

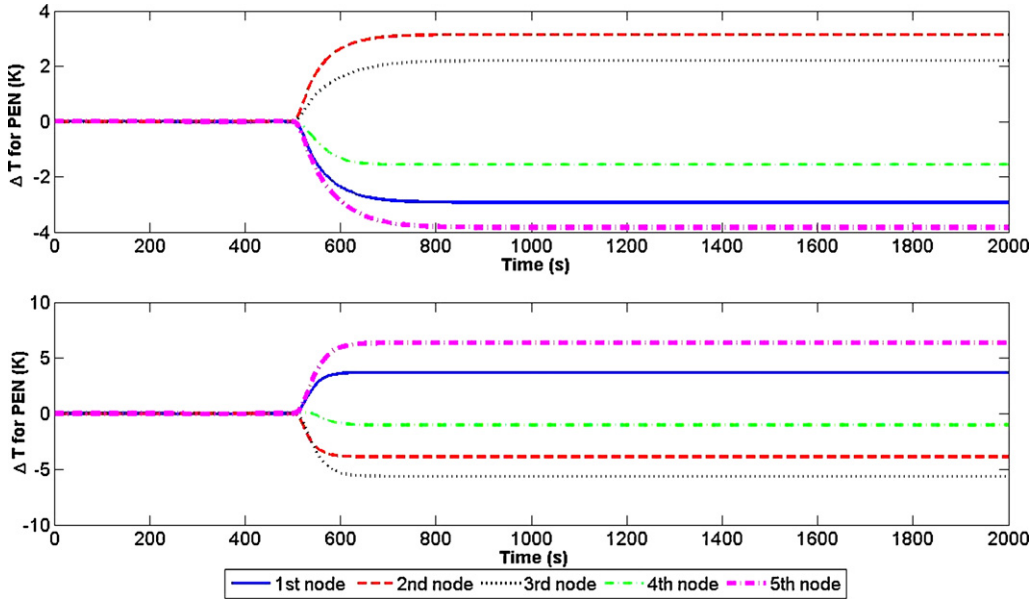

Fig. 9. Closed loop temperature deviation from (top: increasing voltage; bottom: decreasing voltage).

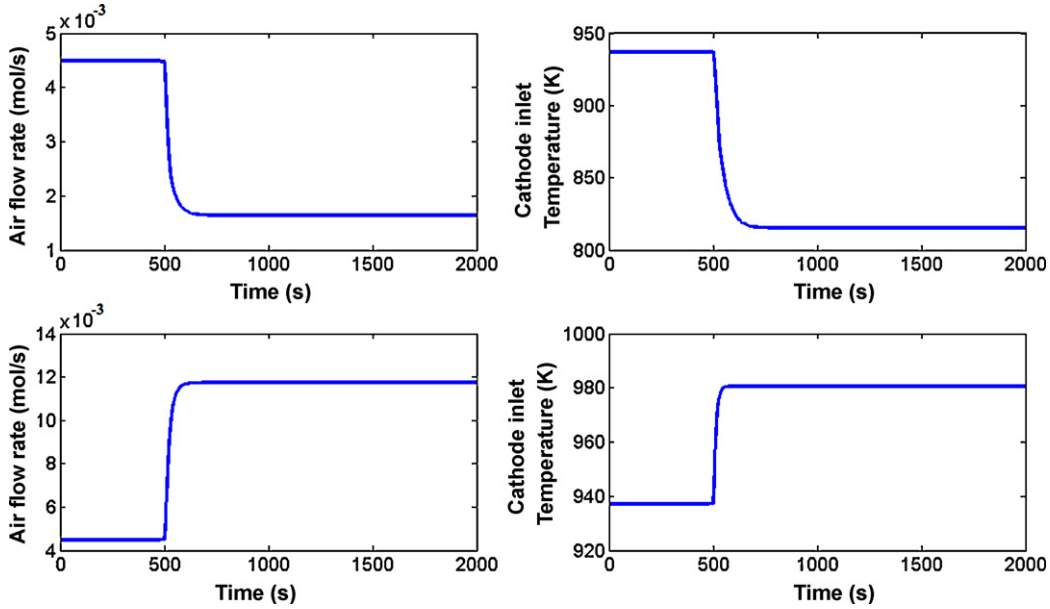

Fig. 10. Inputs during transients (top: increasing voltage; bottom: decreasing voltage).

both actuators into account. One actuator (airflow rate) is used to lower the average temperature, while the second one reduces the spatial variation in temperature by keeping the overall profile close to nominal one. Recall that similar results were obtained when steady-state optimization was used (shown in Table 2). As shown here, a centralized controller, with appropriate cost functionals, results in such a scenario automatically. The actual values obtained in Table 2 are quite close to the ones resulting from feedback controller. Note that the cost functionals used in the two approaches were different and the steady-state optimization used the nonlinear model while the feedback controller was based on the linearized model. The similarity of the results are due to (i) when constant disturbance is introduced, the steady-state values dominate the energy integral (13) making the two optimization objectives similar, (ii) as Fig. 6 showed, the linearized model can capture the effective dynamics over a large envelop.

Figs. 11 and 12 show the evolving temperature profiles as a function of time (Fig. 11) and the spatial variations in the PEN temperature for different voltage changes (Fig. 12). In these figures, the symbols denote the temperatures of nodes 1–5 and the solid lines are used to connect the data point to give a sense of length to the plots. Recall that the temperature of node i is simply the average (and exiting) temperature of that control volume. Points 1 and 5, for example, should not be confused with inlet and exit points of the cell, though the effects of convection is included in finding their (volumetric) average. Given that we are using only 5 segments, the profile looks somewhat coarse and the changes look exaggerated. Overall, the results shown are representative of the physical conditions, with reasonable fidelity.

The open loop result in Fig. 12 (bottom plot) shows that temperature variation has been increased significantly from first node to the last node which can lead to thermal fatigue in fuel cell. On

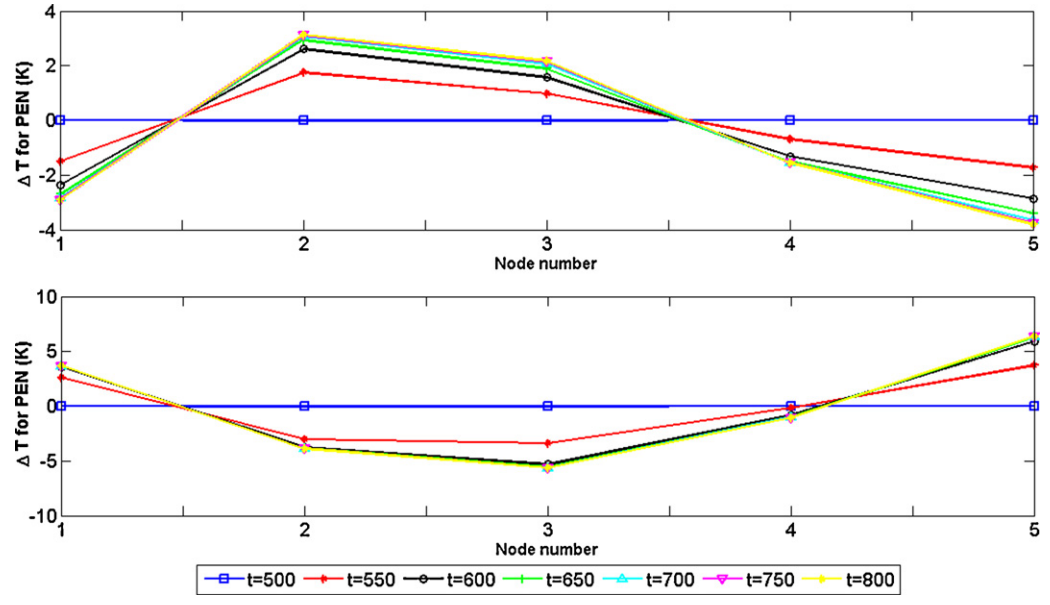

Fig. 11. Change from nominal temperature profile at various time (top: increasing voltage; bottom: decreasing voltage).

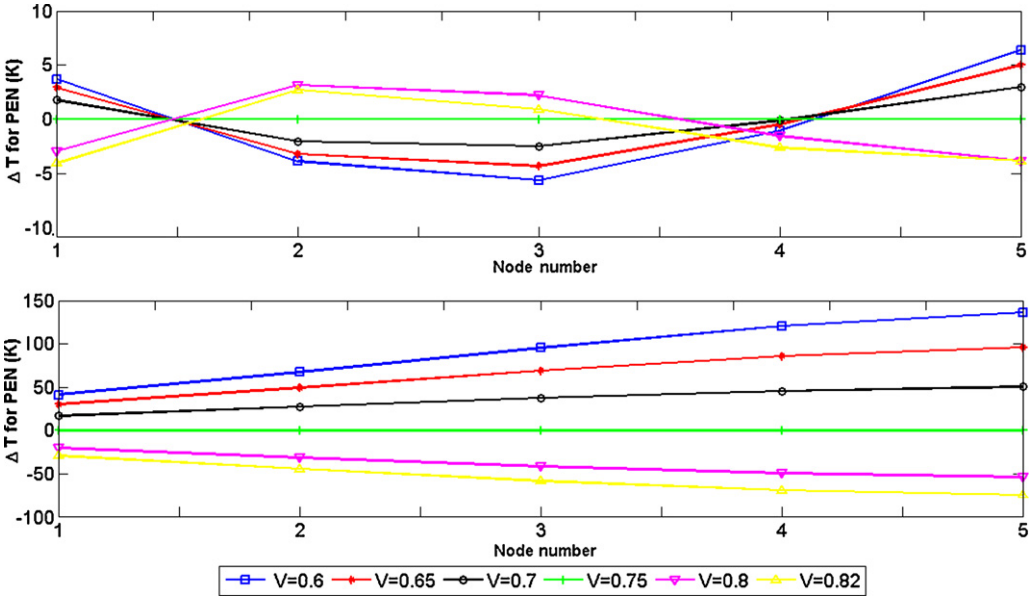

Fig. 12. Change from nominal temperature profile for various voltages (top: closed loop response; bottom: open loop response).

the other hand, output feedback controller tried to minimize the temperature variation and hold it in a much narrower bound.

Next, we evaluate controller performance for the combination of cell voltage increase followed by cell voltage decrease (every 500 s). This combination of disturbance is chosen because of its resemblance to the real fuel cell voltage behavior. Fig. 13 demonstrates the input fuel cell voltage. Fig. 14 shows the absolute value of spatial temperature response for each node with feedback controller for the voltage fluctuation scenario. Fig. 14 shows the absolute temperature to give an overall sense of the magnitude of the temperature variations in time and along the cell, compared to the reference values. The relative changes from the reference values can be deduced easily from the rest of the figures and are not shown here, for brevity.

Comparing Fig. 14 with Fig. 8 shows that the controller reduced the temperature deviation significantly.

Table 5 shows that the controller reduced the variations (in time) of the fuel cell from the nominal profile significantly. These are under the columns denoted by Ni, for *i*th node. The last columns show the max temperature variation (in length) across the fuel cell. This value (as seen from the left extreme of Fig. 14) is 100 K for the nominal 0.75 V case. The closed loops results in a maximum of 186 K of open loops, thus significantly reducing the thermal stress that could have been associated with power change.

Fig. 15 demonstrates the inputs during transients for the controller. When fuel cell voltage decreases, heat generation in the fuel cell will increase, and also on the other hand, when fuel cell voltage increases, heat generation will decrease. The goal of the controller is minimizing the deviation of the spatial temperature from the operating condition. As Figs. 14 and 15 show the extra heat from the fuel cell has been eliminated from the fuel cell through increasing the air flow rate and cathode inlet temperature in case of decreasing voltage. On the other hand, in case of increasing voltage, heat loss from fuel cell has been removed from the fuel cell through decreasing the air flow rate and cathode inlet temperature.

Finally, we discuss the issue of spatial gradient of the fuel cell temperature since that could also be an important consideration. To address this concern, we can adjust the cost functional. For exam-

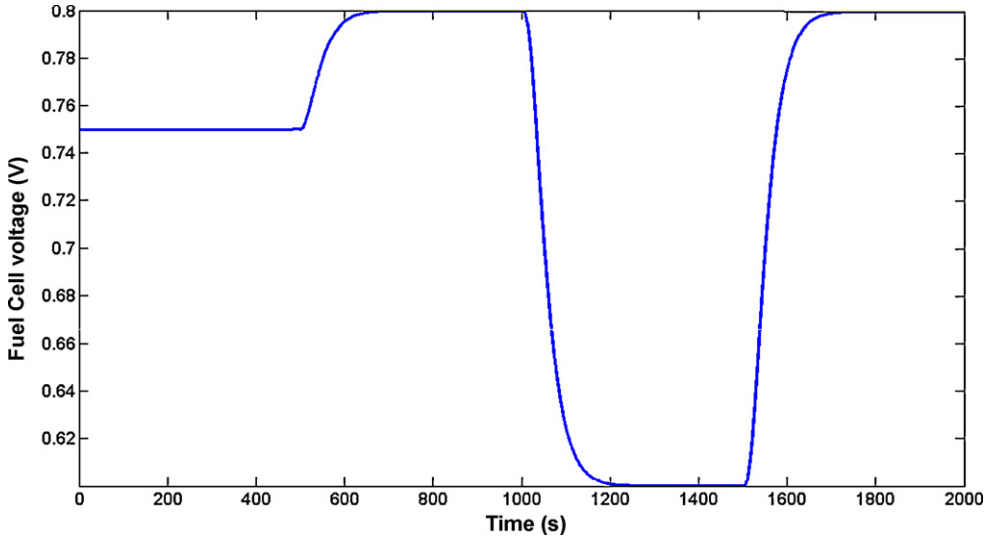

Fig. 13. Change in fuel cell voltage: fluctuating case (disturbance).

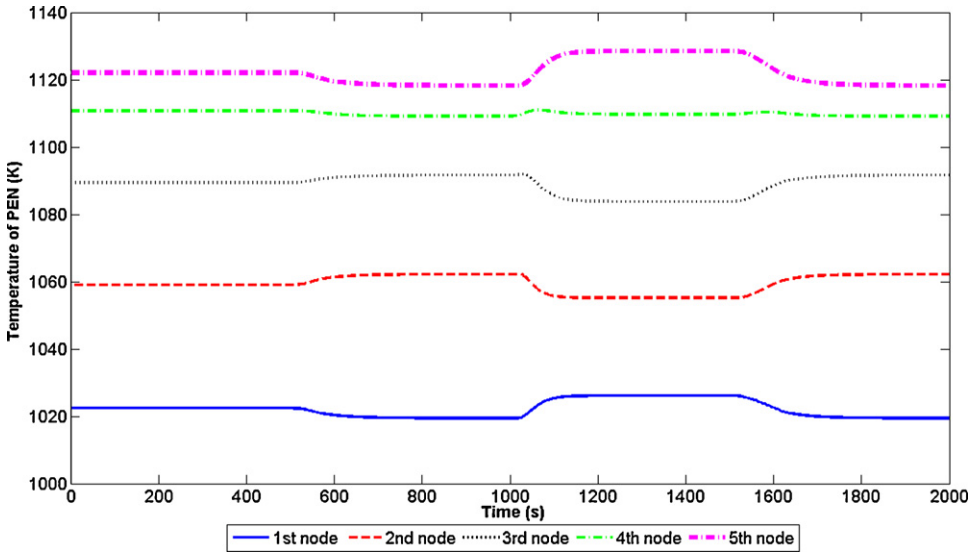

Fig. 14. Temperature response along the cell for the fluctuating voltage case.

Table 5
ΔT from nominal for the fluctuation voltage case.

	ΔT from nominal					Maximum gradient across fuel cell (N_1–N_5)
	N_1	N_2	N_3	N_4	N_5	
Open loop (maximum voltage)	−19.05	−29.4	−38.5	−45.5	−49.3	30.25
Closed loop (maximum voltage)	−2.927	3.14	2.196	−1.554	−3.832	6.972
Open loop (minimum voltage)	37.24	60.8	85.5	108	122.11	84.87
Closed loop (minimum voltage)	3.72	−3.876	−5.635	−1.032	6.385	12.02

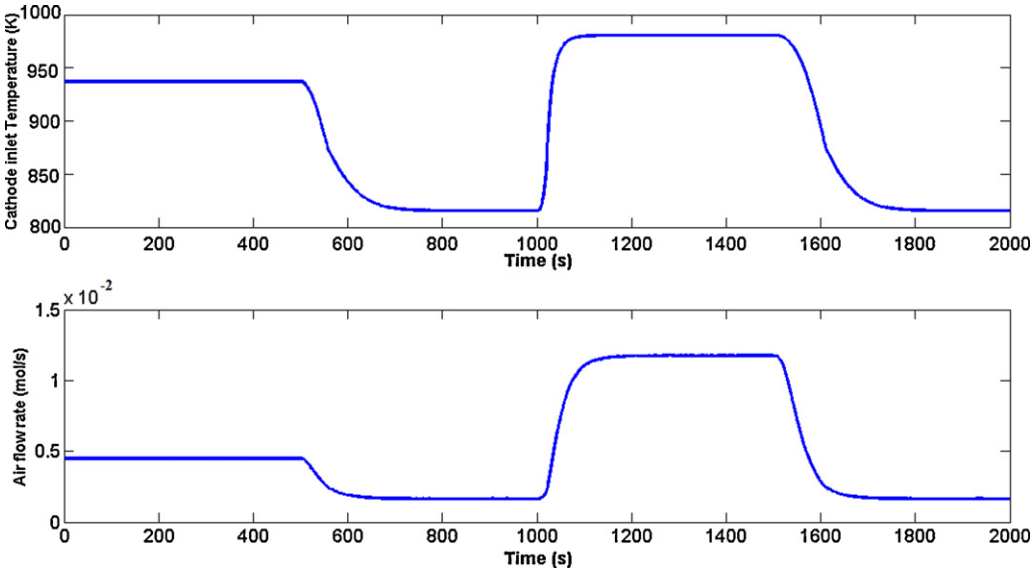

Fig. 15. Controller input during transients for the fluctuating voltage case.

Table 6
Effect of changing cost functional.

	Voltage	Max $\lvert\delta T_i - \delta T_{i-1}\rvert$	Max δT_i	Voltage	Max $\lvert\delta T_i - \delta T_{i-1}\rvert$	Max δT_i
Open loop	0.6	28.2	136.7	0.8	11	−54.02
z		7.59	6.6		6	−3.83
Modified z		8.71	9.32		4.47	5.41
Weighted z		6.9	77.3		3.6	−45.8

ple, we can add $\delta T_i - \delta T_{i-1}$ for $i = 2,3,4,5$ to the control/performance output vector (i.e., z) as an approximation for the gradient of the temperature along the cell. The results are listed in Table 6. The row 'z' corresponds to the δz vector used so far. The row 'modified z' corresponds to the case of having the four $\delta T_i - \delta T_{i-1}$ plus δT_4. The last entry, δT_4, is to hold the overall temperature profile close to the nominal and prevent large drifts. 'Weighted z' in the last row is similar to the 'new z' case, except the entry corresponding to δT_4 is multiplied by 0.1 to place more emphasis on the slope reductions.

The results of Table 6 show that this modification to the cost functional can be used to reduce the peak (or worst case) slope of the temperature along the cell, if that is desired. There is one inconsistency in Table 6, for decreasing fuel cell voltage in the 'Modified z' versus 'z'. Given that the controller here is aimed at reducing the energy (i.e., integral of the square) of the signal, such anomalies can occur. With modest modifications, one can attempt energy to peak or peak-to-peak minimization, but we leave such variations to future work. The exact level of trade-off in the design iterations depends on the specific properties of the fuel cell and is beyond the scope of this paper. It suffices to say that the methodology presented is flexible enough to accommodate such concerns.

6. Conclusion

Controlling SOFC spatial temperature plays an important role in minimizing fuel cell thermal stresses and fatigue. Dynamic modeling has been used to design and evaluate controls in reducing significantly fuel cell spatial temperature variation during load transients. Dynamic modeling provides an effective means to investigate controls without risking loss or deterioration of expensive SOFC systems. The actuation is through manipulating the air flow rate and cathode inlet temperature. The control technique is a basic H-infinity output feedback design, developed for a reduce-order linearized model of the fuel cell, around a baseline operating condition. This control technique is shown to be quite effective in reducing the thermal variations, due to changes in the power demand, while a variety of other disturbances (e.g., fuel variations) can easily be addressed but are left to future work. Similarly systematic approaches aimed at reducing peak response (e.g., error or variations) to peak or energy bounded disturbance can also be attempted with relative ease. Simulated control results indicate for the first time that future SOFC systems can be designed and controlled to have superb load following characteristic with less than previously expected thermal stresses.

References

[1] S. Chalk, American Recovery and Reinvestment Act Program Plan for the Office of Energy Efficiency and Renewable Energy, Department of Energy, The Office of Energy Efficiency and Renewable Energy (EERE), 2009.
[2] E. Sison-Lebrilla, G. Kibrya, V. Tiangco, D. Yen, P. Sethi, M. Kane, Research Development and Demonstration Roadmap, California Energy Commission PIER Renewable Energy Technologies Program, CEC-500-2007-035, Sacremento, 2007, 45 pp.
[3] A. Cano, F. Jurado, Optimum Location of Biomass-Fuelled Gas Turbines in An Electric System, 2006, 6 pp.
[4] F. Mueller, F. Jabbari, R. Gaynor, J. Brouwer, Journal of Power Sources 172 (1) (2007) 308–323.
[5] F. Mueller, R. Gaynor, A.E. Auld, J. Brouwer, F. Jabbari, G.S. Samuelsen, Journal of Power Sources 176 (1) (2008) 229–239.
[6] F. Mueller, Journal of Power Sources 187 (2) (2009) 452–460.
[7] F. Mueller, B. Tarroja, J. Maclay, F. Jabbari, J. Brouwer, S. Samuelsen, Design, Simulation and Control of a 100 Megawatt Class Solid Oxide Fuel Cell Gas Turbine Hybrid System, ASME, Denver, Colorado, 2008.
[8] F. Mueller, The Dynamics and Control of Integrated Solid Oxide Fuel Cell Systems: Transient Load-Following and Fuel Disturbance Rejection, University of California, Irvine, Irvine, 2008 (Doctorate).
[9] A.M. Murshed, B. Huang, K. Nandakumar, Estimation and control of solid oxide fuel cell system, Computers and Chemical Engineering 34 (2010) 96–111.
[10] M.C. Williams, J.P. Strakey, W.A. Surdoval, L.C. Wilson, Solid State Ionics 177 (19–25) (2006) 2039–2044.
[11] M.F. Serincan, U. Pasaogullari, N.M. Sammes, A transient analysis of a micro tubular solid oxide fuel cell (SOFC), Journal of Power Sources 194 (2009) 864–872.
[12] A. Nakajo, C. Stiller, G. Harkegard, O. Bolland, Journal of Power Sources 158 (1) (2006) 287–294.
[13] A. Nakajo, Z. Wuillemin, J. Van herle, D. Favrat, Journal of Power Sources 193 (1) (2009) 203–215.
[14] Y.C. Hsiao, J.R. Selman, Solid State Ionics 98 (1–2) (1997) 33–38.
[15] F. Mueller, F. Jabbari, J. Brouwer, R. Roberts, T. Junker, H. Ghezel-Ayagh, Journal of Fuel Cell Science and Technology 4 (2007) 221–230.
[16] C. Stiller, B. Thorud, O. Bolland, R. Kandepu, L. Imsland, Journal of Power Sources 158 (1) (2006) 303–315.
[17] R. Gaynor, F. Mueller, F. Jabbari, J. Brouwer, Journal of Power Sources 180 (1) (2008) 330–342.
[18] B.A. Haberman, J.B. Young, International Journal of Heat and Mass Transfer 48 (25–26) (2005) 5475–5487.
[19] H.-K. Park, Y.-R. Lee, M.-H. Kim, G.-Y. Chung, S.-W. Nam, S.-A. Hong, T.-H. Lim, H.-C. Lim, Journal of Power Sources 104 (1) (2002) 140–147.
[20] P.-W. Li, M.K. Chyu, Journal of Power Sources 124 (2) (2003) 487–498.
[21] J. Yang, X. Li, H.-G. Mou, L. Jian, Journal of Power Sources 193 (2) (2009) 699–705.
[22] J. Yang, X. Li, H.-G. Mou, L. Jian, Journal of Power Sources 188 (2) (2009) 475–482.
[23] A. Nakajo, Z. Wuillemin, J. Van herle, D. Favrat, Journal of Power Sources 193 (1) (2009) 216–226.
[24] Y. Inui, N. Ito, T. Nakajima, A. Urata, Energy Conversion and Management 47 (15–16) (2006) 2319–2328.
[25] R. Roberts, J. Brouwer, F. Jabbari, T. Junker, H. Ghezel-Ayagh, Journal of Power Sources 161 (1) (2006) 484–491.
[26] Y. Kuniba, Development and Analysis of Load Following SOFC/GT Hybrid System Control Strategies for Commercial Building Applications, University of California, Irvine, Irvine, 2007.
[27] T. Kaneko, J. Brouwer, G.S. Samuelsen, Journal of Power Sources 160 (1) (2006) 316–325.
[28] J. Brouwer, F. Jabbari, E.M. Leal, T. Orr, Journal of Power Sources 158 (1) (2006) 213–224.
[29] K. Min, J. Brouwer, J. Auckland, F. Mueller, S. Samuelsen, Dynamic Simulation of a Stationary PEM Fuel Cell System, ASME, Irvine, CA, 2006.
[30] F. Mueller, J. Brouwer, F. Jabbari, S. Samuelsen, Dynamic Simulation of an Integrated Solid Oxide Fuel Cell System Including Current-Based-Fuel Control, 2005 May 23–25, ASME, Ypsilanti, MI, 2005, pp. 1–11.
[31] F. Mueller, J. Brouwer, S. Kang, H.-S. Kim, K. Min, Journal of Power Sources 163 (2) (2007) 814–829.
[32] R. Roberts, A Dynamic Fuel Cell-Gas Turbine Hybrid Simulation Methodolgy to Establish Control Strategies and an Improved Ballance of Plant, University of California, Irvine, Irvine, 2005, 338 pp. (Doctorate).
[33] R. Roberts, J. Brouwer, Journal of Fuel Cell Science and Technology 3 (1) (2006) 18–25.
[34] S. Campanari, P. Iora, Journal of Power Sources 132 (1–2) (2004) 113–126.
[35] J. Xu, G.F. Froment, AIChE Journal 35 (1) (1989) 88–96.
[36] J. Xu, G.F. Froment, AIChE Journal 35 (1) (1989) 97–103.
[37] J.-W. Kim, A. Virkar, K.-Z. Fung, M. Karum, S. Singhal, Journal of The Electrochemistry Society 146 (1) (1999) 69–78.
[38] T. Iwasaki, R.E. Skelton, Automatica 30 (8) (1994) 1307–1317.
[39] K. Zhou, J.C. Doyle, Essentials of Robust Control, Prentice Hall, 1998.
[40] S. Boyd, L.E. Ghaoui, E. Feron, V. Balakrishnan, Linear Matrix Inequalities in System and Control Theory, 1994.
[41] P. Gahinet, P. Apkarian, International Journal of Robust and Nonlinear Control 4 (4) (1994) 421–448.
[42] C. Scherer, P. Gahinet, M. Chilali, IEEE Transaction on Automatic Control 42 (7) (1997) 896–911.
[43] R.E. Skelton, T. Iwaskai, K. Grigoriadis, A Unified Algebraic Approach to Linear Control Design, Taylor and Francis, London, 1998.
[44] P. Gahinet, A. Nemirovski, A.J. Laub, M. Chilali, LMI Control Toolbox for Use with Matlab, The MathWorks, Inc., 1995.